DPIV- measurements of the flow field in a micro-axial blood pump

Michael Triep[1], Christoph Brücker[1], Thorsten Sieß[2]

1: Institut für Mechanik und Fluiddynamik, TU Freiberg, Germany, Michael.Triep@imfd.tu-freiberg.de
1: Institut für Mechanik und Fluiddynamik, TU Freiberg, Germany, Christoph.Bruecker@imfd.tu-freiberg.de
2: Impella CardioSystems GmbH, Aachen, Germany, tsiess@impella.com

Abstract. In the 1990's miniaturization technology has arrived at a stage where miniature left ventricular assist devices (VAD's) with an integrated motor became feasible. This led to a 12 French microaxial blood pump concept for the support of the left ventricle without having to conduct a thoracotomy. To comply with medical demands of a sufficient flow output at physiological pressure load conditions these pumps have to be run at high rotation speeds where hemolysis and thrombogenecity may become very important. These will determine the duration of implementation. In the present study the flow through a micro-axial blood pump is analyzed in-vitro by means of digital particle image velocimetry (DPIV) using a hydraulic mock circuit with a transparent test chamber. The geometric configuration of the test chamber and the micro-axial blood pump correspond to the situation after implementation of the pump system in the human body. Phase locked DPIV recordings were done in the axial centerplane and in parallel planes with an axial offset. The results show no indication of flow separation at the blades for the nominal working conditions. The regions of high vorticity are detected and the path of the tip clearance vortices, was reconstructed. The results confirm the choice of a two-blade impeller as the most appropriate during the early design process. Furthermore, the influence of the pump housing at the outlet region is analyzed.

1. Introduction

Nowadays there exist a vast variety of blood pumps for cardiac support (Reul et al. 2004). They may be grouped as in the classical way into displacement and rotary pump systems. The rotary pumps themselves can be divided into three types: axial, mixed-flow and centrifugal type pumps. The first two types have a great potential for applications in medical instruments in keyhole-surgery, since they can be miniaturized to a greater extent. Small rotary pump systems have been developed for the treatment of patients with cardiac insufficiency as well as for applications in intra- and extra-corporal circulation. From the late 1980's until the 1990's a first small catheter-mounted intraaortic left-ventricular axial blood pump with extracorporal motor has been for a short time in the market, the Hemopump (Wampler et al. 1988, Frazier et al. 1990). This concept of catheter-mounted pumps was picked up by Sieß (1998) who developed a small micro-axial blood pump with an integrated motor with an overall outer diameter of 4 mm, which is placed with a catheter via the arteria femoralis into the left ventricle. Any hemodynamical and fluid mechanical optimization of such a pump will extend substantially the period of pump implementation which is of great significance and impact for cardiology, the patients and the health care system.
The aim of the flow studies in these micro-axial blood pumps is, in effect, the search of an optimal trade-off between the hydraulic efficiency and the minimization of blood traumatisation and thrombus formation. Due to the high rotational speeds the shear stresses may locally become very high, the secondary flow field may evolve in a very complex manner and red blood cells residence times in recirculation and high shear zones may become important. Therefore, an experimental flow study of micro-axial blood pumps is indispensable also in view of the validation of computational fluid dynamical (CFD) simulations. The micro-axial pump system is described in section 2. Thereafter, the experimental setup, including the hydraulic mock circuit and the experimental

technique of phase-locked DPIV, are described. Finally, the most important results concerning the micro-axial blood pump are presented and discussed.

2. The micro-axial blood pump

The Impella acute micro-axial blood pump has an overall outer diameter of 4 mm and is integrated in a 12 French catheter, which is placed via the femoral artery into the left ventricle (Fig. 1). A flexible cannula (Fig. 2) guarantees the smooth insertion through the arch of the aorta and the aortic valve. The two-bladed impeller which is shown in Fig. 3 is powered by an integrated motor which is supplied electronically from outside with a control unit. The curvature of the blades that have a constant thickness follows a specific function. The blade enlacement, as can be seen, is slightly greater than 90°.

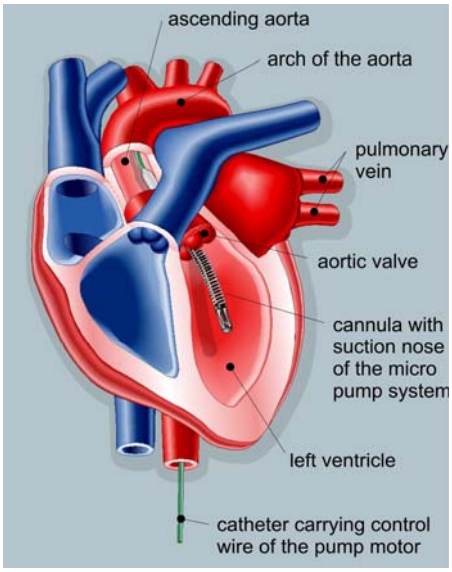

Fig. 1 Implementation of the acute pump system into the left ventricle

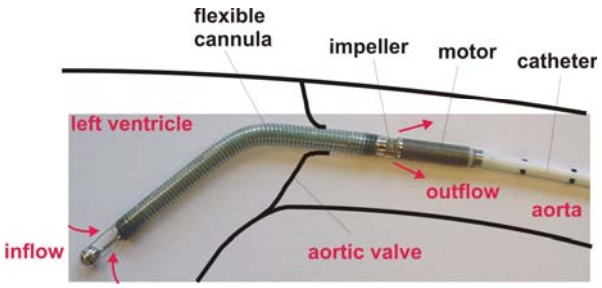

Fig. 2 The photograph shows the left ventricular micro-axial blood pump (Impella CardioSystems AG, Aachen, Germany) including the motor and the inflow cannula (diameter 4mm)

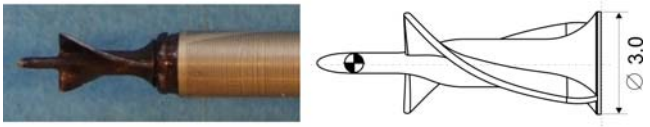

Fig. 3 Impeller without housing; geometric dimensions

The pump's housing is fixed to the motor with 5 struts, which unavoidably will act like an obstacle in the outflow. The impeller shown in Fig.3 represents already the optimized version, which will be explained further below. The pump in its initial design circulated a maximum blood flow of 2.4 ltr/min at 50 mmHg at rotational speeds of 50.000 rpm. At higher rotation speeds the blood undergoes a dramatic increase of the hemolysis. The major aim of the present work was to improve the pump efficiency to achieve the same discharge at lower rotational speeds (Fig. 4) and thus decreased levels of hemolysis and, therefore to maximize the running period in the patient. The most promising and feasible improvement could be achieved with an impeller design leaned upon aerodynamic drag reduction experiences. It is known that the drag of an axisymmetric body can be reduced in some cases by a forebody, which is most effective in turbulent flows. The drag reduction is mainly due to the redistribution of the wall shear stress (higher wall shear along the nose with a small effective area, lower shear stress along the main body with a much larger effective surface area) and the stabilization of the boundary layer in the successive convex parts of the nose as described by Bandyopadhyay (Fig. 5). The achieved optimization allows operating the pump at reduced rotational speeds of 45.000 rpm while producing the same flow rate as the original pump at 50.000 rpm and, in effect, at much lower hemolysis levels.

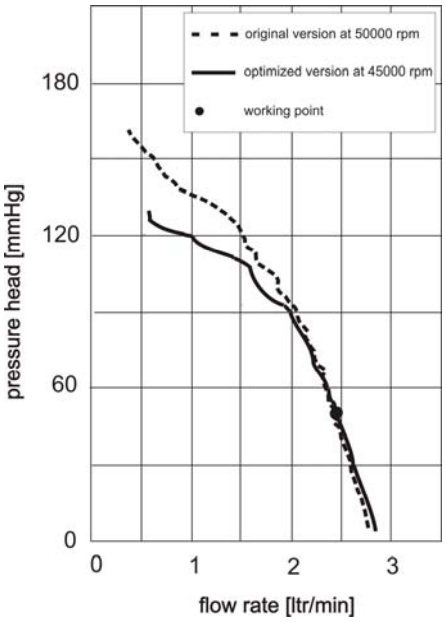

Fig. 4 Performance curves for the original and optimized impeller at 50000 rpm and 45000 rpm, respectively

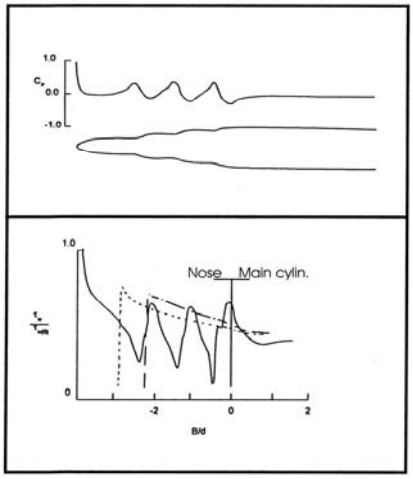

Fig. 5 Concept of drag reduction (Bandyopadhyay, 1989) (top): The three-stage nose body and its computed surface pressure distribution, (bottom): Computed wall-shear-stress distribution in the three-stage nose body (solid line) compared with those of equivalent-area (dashed line) and equivalent-volume (chain line) half-elliptic noses

3. Experimental set-up

The experimental setup (Fig. 6) consists of a hydraulic setup, including the micro-axial blood pump system, an optical setup, and the digital imaging and processing system.

3.1 The flow circuit

The impeller is integrated into a hydraulic mock loop with a fully transparent Perspex housing of the pump (Fig. 7). A newtonian water/glycerine mixture (35 weight % glycerine) with a density of 1060 kg/m^3 and a viscosity of 3.6 cP at a temperature of 21°C is used as working fluid. Flow rate is controlled by an ultrasound flow meter and the pressure load is regulated by a throttle valve downstream of the pump. The connector of the impeller to the mock circuit allows an easy change of different impeller types.

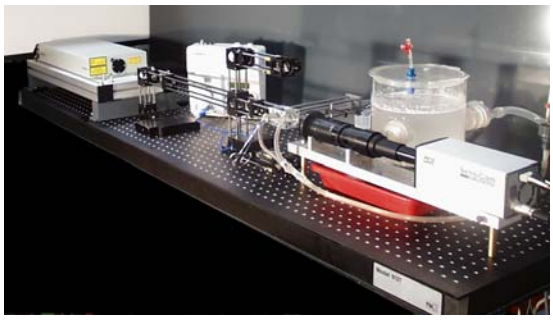

Fig. 6 Photograph of the setup

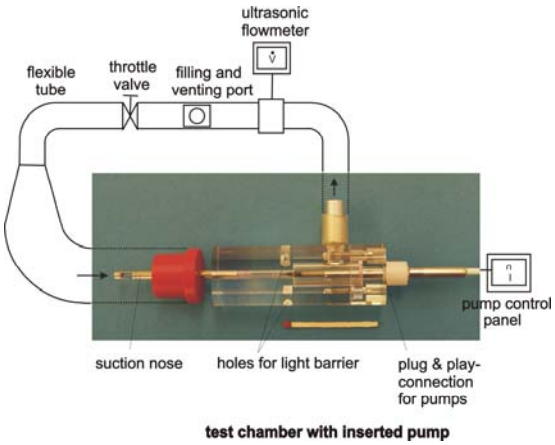

Fig. 7 Flow circuit for pump tests

3.2 Optical arrangement

The technique of phase-locked DPIV is used to capture the flow field at any desired angular phase position φ of the impeller. The laser beam of a Nd:Yag pulse laser (Photonics, Edinburgh, UK) with a power of 30 mJ/pulse is expanded and focused to a 0.2 mm light sheet. A prism system redirects the sheet from top and bottom into the test chamber. A micro-positioning stage allows moving the test chamber through the light-sheet with high precision. The full optical arrangement can be seen in Fig. 8.

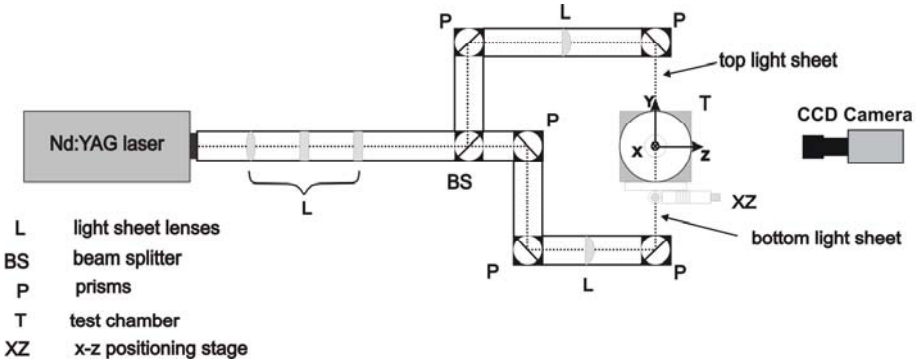

Fig. 8 Optical arrangement (Brücker et al. 2002)

The flow is seeded with fluorescent tracer particles (Dantec Dynamics A/S, Skovlunde, Denmark) with a mean diameter of 5 microns in a concentration of 0.6 g/liter. An orange filter (LOT-Oriel GmbH&Co KG, Darmstadt, Germany) eliminates most of the disturbing wall reflections so that near-wall regions are better resolved (Fig. 9). A telecentric lens (SILL Optics GmbH&Co KG, Wendelstein, Germany) with a fixed magnification of 1.422 is used in combination with a CCD sensor (1280 by 1024 pixels, double-shutter PCO Sensicam PCO AG, Kelheim, Germany) to record the particle images in the light sheet. The pulse separation is 10 μs. An infrared light barrier positioned with an axial offset at the leading edge of the impeller blades (Fig. 10) allows synchronizing the laser pulse to any desired angular phase position of the impeller. A Labview controller console in combination with a counter card (National Instruments, Austin, TX, USA) is used for the phase locked recording. The angular precision of the synchronization in this setup is ±1°.

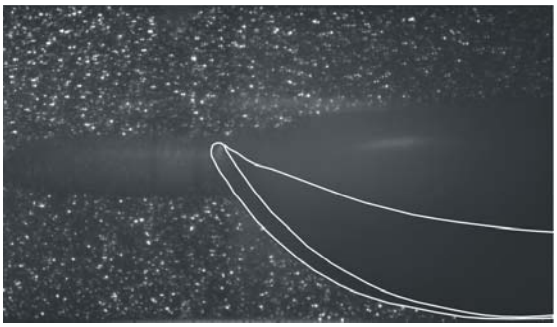

Fig. 9 Exemplar double-exposed particle image of the impeller region; impeller blade outlined

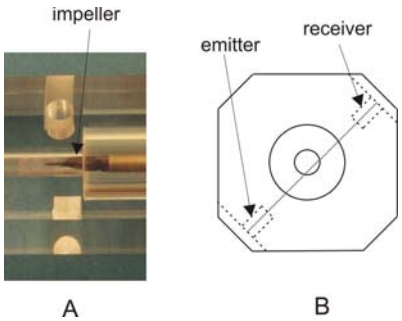

Fig. 10 Side view (A) and front view (B) of the position of the holes for the infrared light barrier

Measurements were taken in the axial centerplane and in parallel planes with an axial offset. In the post-processing the obstructed regions by the rotor are masked in order to get a better image contrast near the walls.

Velocity fields are calculated by cross-correlation procedure with window shifting and window refinement technique. The particle density is high enough to achieve high quality vector fields with 32 by 32 interrogation areas. Therefore, the finest resolved structures in the flow field are of the order of D/46, D being the inflow inner cannula diameter of 3.7 mm. The results given below represent averages of 50 DPIV recordings at the same angular phase position. The velocity profiles are reconstructed at different axial locations in main flow direction and around the impeller blades in a co-rotating frame of reference. Furthermore, the vorticity is extracted from the velocity field.

4 Results

The results obtained in this study are ordered as follows; first, the velocity profiles in the axial centerplane are shown and compared to CFD results; next, the regions of concentrated vorticity in the impeller region are characterized; further, the flow near the blades is studied. Finally, the influence of the impeller housing on the outflow is discussed. The working conditions for the pump are n = 45000 rpm, Q = 2.4 ltr/min and Δp = 50 mmHg.

4.1 Measurements in the axial centerplane

Velocity flow profiles

The velocity flow profiles obtained by DPIV in a centerplane are shown in dashed lines in Fig. 11. Phase position 0° corresponds to the position of the rotor where the leading edge of the blades is horizontal, e.g. where it is aligned in direction normal to the paper plane. The velocity profiles shown in solid lines in Fig. 11 correspond to the results obtained by a CFD simulation with exactly the same geometry and boundary conditions as in the experimental case.

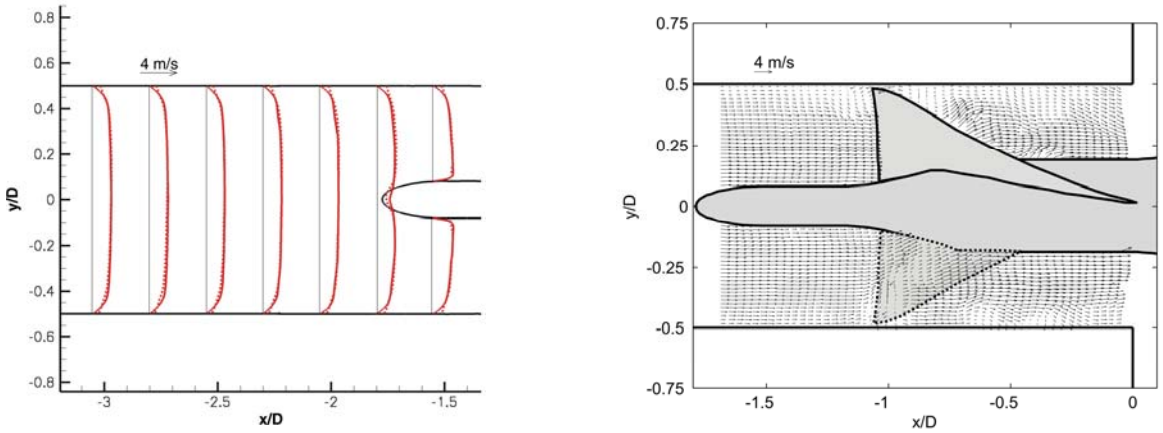

Fig. 11 Mean axial velocity profiles of inflow: DPIV (dashed line); CFD simulation (solid line) (*left*), instantaneous flow field in impeller region (*right*)

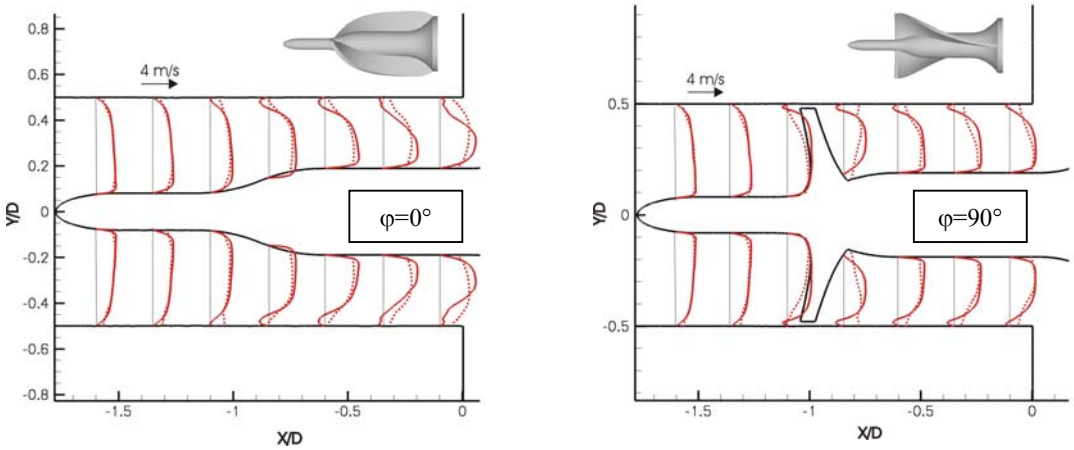

Fig. 11 (cont'd) Mean axial velocity profiles in impeller region: DPIV (dashed line); CFD simulation (solid line)

The profiles show a fully developed turbulent inflow as encountered in the real inflow cannula for this working point with maximum flow velocities along the centreline of 4.5 m/s. The Reynolds number based on the diameter D is 3670. The flow is decelerated near the stagnation point of the hub and forms boundary layers with steep gradients near the wall. The mean axial velocity profiles along the impeller show a good qualitative and quantitative agreement between experiment and CFD, especially in regions of core flow. In regions with very high velocity gradients a discrepancy between the PIV and CFD results is seen. One reason may be the limitations of conventional PIV in regions with high shear or strong out-of-plane motion. The gradients are low pass filtered by the finite extension of the interrogation windows (Adrian 1991). The use of micro PIV (Meinhart et al. 1999) could resolve the details of the velocity field in the boundary layer regions with higher accuracy. Despite these discrepancies it is remarkable that under these conditions of very small geometries and for extremely high rotational speeds of 45.000 rpm the mean axial velocity profiles in the numerical simulation and the experiments agree quite well. An exemplar instantaneous flow field is also shown in Fig. 11.

Circumferential vorticity distribution in the impeller region

Fig. 12 shows the evolution of the flow in angular phase steps of 18° in the impeller region of the optimized pump design. The solid and dashed lines highlight regions of concentrated vorticity shown as isolines of the positive and negative circumferential vorticity component, respectively. The vorticity is normalized with the angular speed of the impeller $\omega_{impeller}$. It is clearly visible that the upper tip clearance vortex has a stronger presence in the x-y-plane in phase positions 144°, 162° and 0°, whereas the lower tip clearance vortex is strong in phase positions 18°, 36° and 54°. The axis of the tip clearance vortex is tilted as the vortex moves downstream. At its origin close to the leading edge of the blade the axis is more or less perpendicular to the x-y-plane and becomes parallel to it during its backward drifting. The 3-D path of the tip clearance vortex has been reconstructed by interpolating the vortex position data from Fig. 12 (indicated by A, B, C, D and E) and assuming a constant vortex diameter of 0.1D. It is shown in Fig. 13 as seen on a co-rotating frame of reference.

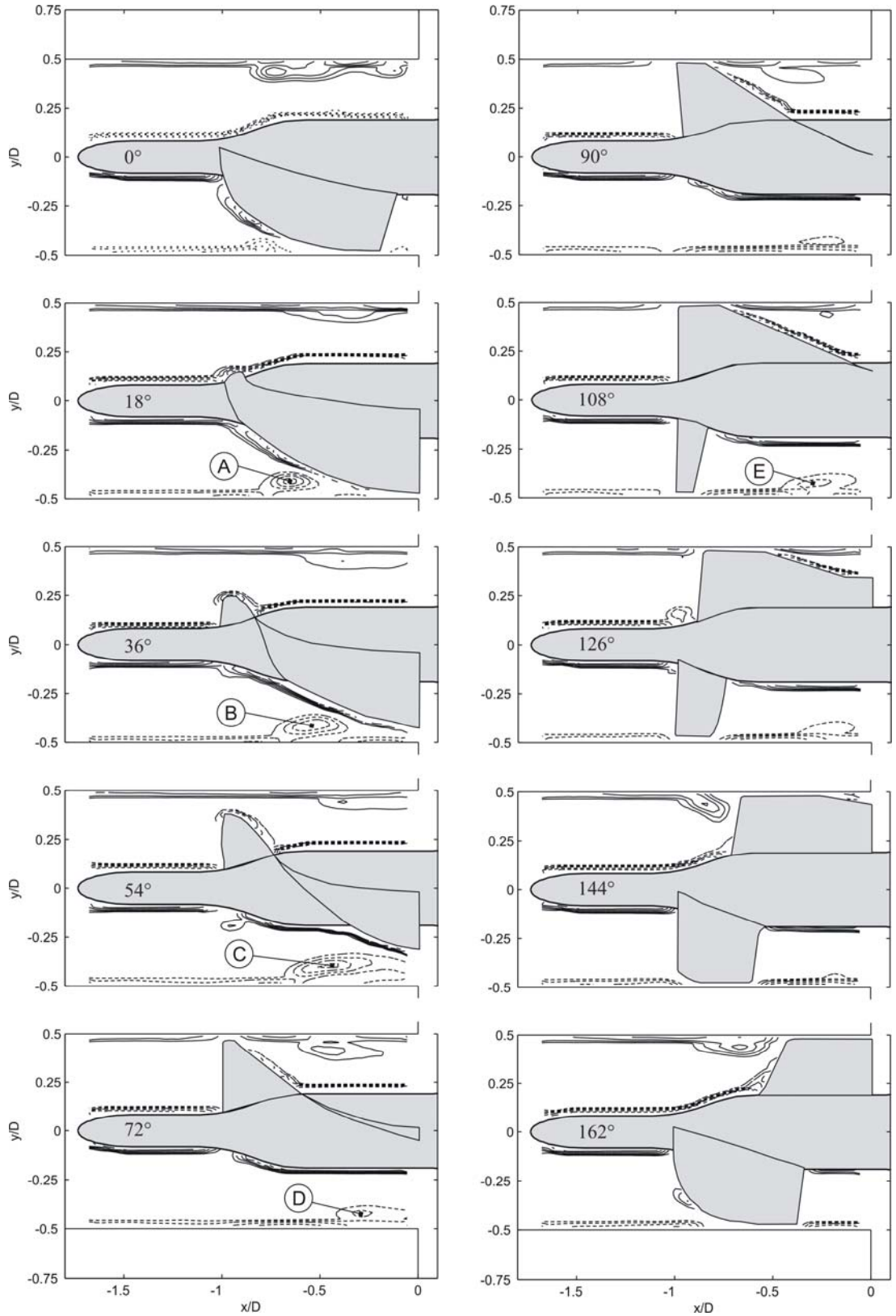

Fig. 12 Evolution of the flow structure in the centerplane over one revolution of the impeller in steps of 18°. The solid and dashed lines indicate the isolines of the positive and negative circumferential vorticity component, respectively. The isolines start with an absolute value of $\omega/\omega_{impeller}$ of 1 with increments of 0.5.

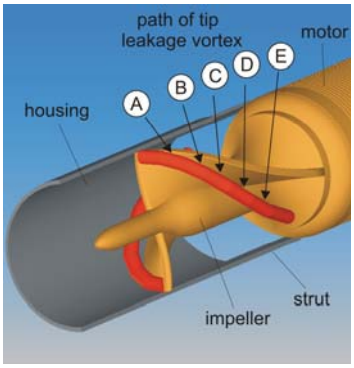

Fig. 13 Cut view of the inflow cannula and the pump housing showing the impeller and the path of the tip leakage vortex as seen on a co-rotating frame of reference

Fig. 13 clarifies that the tip clearance vortex as it moves downstream drifts from the blade. It becomes visible that even at a pressure load of 50 mmHg and a high rotational speed of 45.000 rpm the vortex path will not be intercepted by the second blade on its passage. This is a confirmation for the choice of a 2-blade impeller as the most appropriate under such conditions. This impeller promises to have a better hemolytic performance than a 3- or 4-bladed rotor, for which one would expect a higher blood traumatization due to the repeated interaction of the leading edges with the tip clearance vortices.

4.2 Measurements in planes parallel to the axial centerplane

From theory it is known that the profile of the impeller's blade has a direct influence on the pump's output. Therefore, off-axis measurements were carried out in order to get an idea of the flow field near the blades. A meridional slice would be the ideal surface on which to determine the flow around the blades. We are restricted here to a planar light sheet which makes it impossible to capture accurately the flow around the entire blade all at once. We therefore recorded the flow at two different angular phase positions and with two respective offsets z to the axial centerplane. These are shown in Fig. 14. The velocity profiles around the blades give no indication of flow separation.

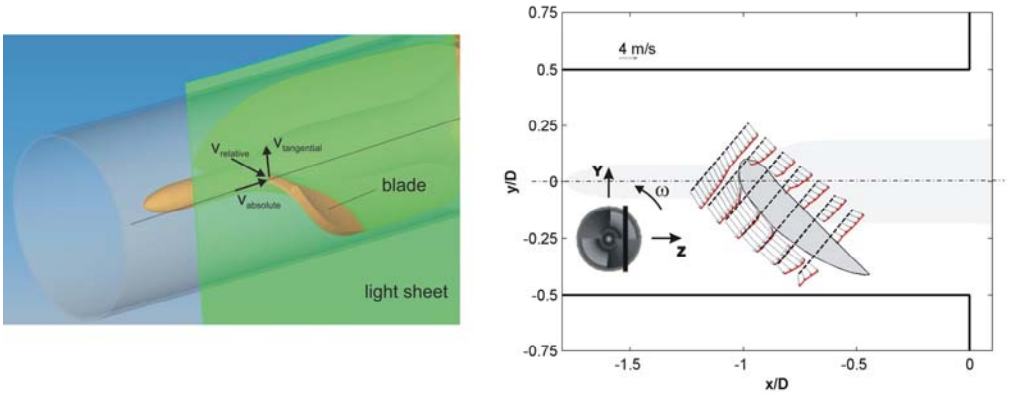

Fig. 14 Flow around the impeller blades at z = 1.0 mm and φ = 0°

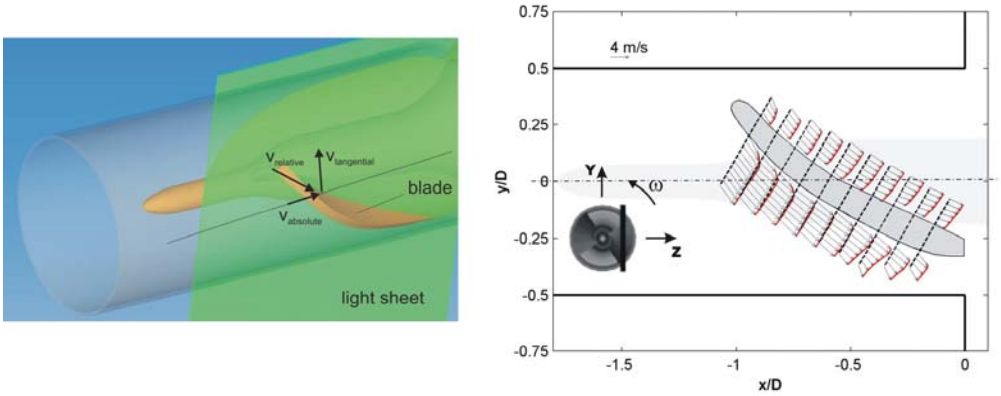

Fig. 14 (cont'd) Flow around the impeller blades at z = 1.2 mm and φ = 36°

4.3 Influence of the impeller housing on the outflow

In Fig. 15 two instantaneous PIV images of the flow at the outflow region in the gap between two struts (A) and behind a strut (B) of the impeller housing are shown. The outlet chamber simulates the annular flow region downstream in the aorta. It can be seen that for the case of the flow between the housing struts this region experiences a recirculation that influences the outflow in a positive way. A bypass flow due to residual systolic heart activity as in reality would not affect the flow through the impeller, but it would keep the discharge of the pump wall-bounded for a long period and thus enhance the cooling of the integrated motor. The maximum velocities can reach values up to the threefold the mean inflow velocity. The flow field here is highly turbulent and stochastic. The flow in a plane behind one housing strut evidences as to be expected a von-Kármán-like vortex street.

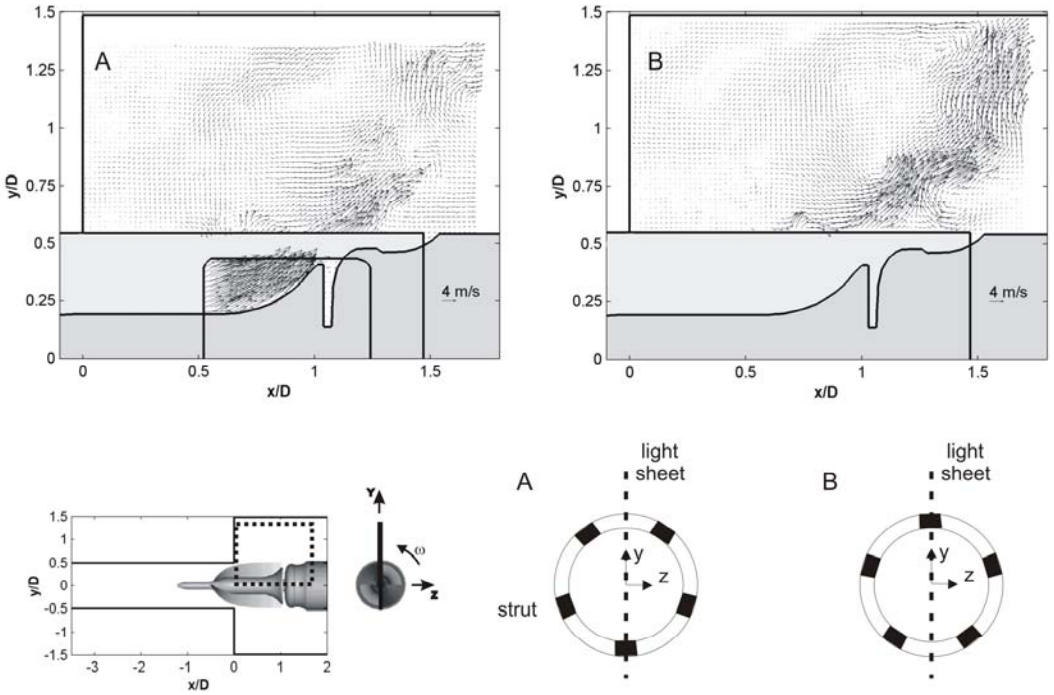

Fig. 15 Instantaneous PIV images of the flow at the discharge region in the gap between two struts (*A*) and behind a strut (*B*) of the impeller outlet cage

5 Conclusion and outlook

The knowledge of the entire flow field through a micro-axial blood pump is indispensable in order to locate possible flow separations, recirculation areas, secondary flows and regions of high shear stress. These flow features can have a big impact on the duration of usage of such devices and in the compliance of regulations imposed by public authorities. The flow field determines to a great extent the hemolytic and thrombogenic performance of the pump system.
In this paper the flow through a micro-axial blood pump was studied by means of phase-locked DPIV. This measurement technique has proven to be an ideal design tool for the optimization of the impeller blades and hub even at the extreme conditions encountered in this study such as the small size of the pump and the high rotational speeds.
The mean axial velocity profiles showed a good agreement with CFD simulation results. From the vorticity data the drifting paths of the tip leakage vortices could be reconstructed. From this, we could observe that the subsequent blade does not intercept the tip leakage vortex generated by the anterior blade. The flow around the blades showed no separation. Finally, the flow field in the discharge region has been visualized, in particular, showing the effect of the outlet cage's struts.

References

Adrian RJ (1991) Particle-Imaging techniques for experimental fluid mechanics. Ann. Rev. of Fluid Mech. 23:261-301

Bandyopadhyay P (1989) Convex Curvature Concept of Viscous Drag Reduction. In: Bushnell DM, Hefner JN (eds) AIAA Progress in Astronautics and Aeronautics, 123:285-324

Brücker C, Schröder W, Apel J, Reul H, Sieß T (2002) DPIV study of the flow in a microaxial blood pump. Proceedings of the 9th Symposium on Transport Phenomena and Dynamics of Rotating Machinery, ISROMAC-9, Honolulu, Hawaii, USA

Frazier OH, Wampler RK, Duncan, Dear WE, Macris MP, Parnis SM, Fuqua JM (1990) First human use of the Hemopump, a catheter-mounted ventricular assist device. The Annals of Thoracic Surgery 49:299-304

Meinhart CD, Werely ST, Santiago JG (1999) PIV measurements of a microchannel flow. Exp. in Fluids 27:414-419

Reul H, Akdis M (2004) Temporary or permanent support and replacement of cardiac function. Expert Review of Medical Devices 1(2):215-227

Sieß T (1998) Systemanalyse und Entwicklung intravasaler Rotationspumpen zur Herzunterstützung. Ph.D. thesis, Faculty of Mechanical Engineering, RWTH Aachen

Wampler RK, Moise JC, Frazier OH, Olsen DB (1988) In vivo evaluation of a peripheral vascular access axial flow blood pump. ASAIO Trans 34(3):450-4